Video Article

Quantitative Optical Microscopy: Measurement of Cellular Biophysical Features with a Standard Optical Microscope

Kevin G. Phillips[1,2], Sandra M. Baker-Groberg[1], Owen J.T. McCarty[1,3]

[1]Department of Biomedical Engineering, Oregon Health & Science University, School of Medicine

[2]Department of Dermatology, Oregon Health & Science University, School of Medicine

[3]Department of Cell & Developmental Biology, Division of Hematology & Medical Oncology, Knight Cancer Institute, Oregon Health & Science University, School of Medicine

Correspondence to: Kevin G. Phillips at phillkev@ohsu.edu

URL: https://www.jove.com/video/50988
DOI: doi:10.3791/50988

Keywords: Bioengineering, Issue 86, Label-free optics, quantitative microscopy, cellular biophysics, cell mass, cell volume, cell density

Date Published: 4/7/2014

Citation: Phillips, K.G., Baker-Groberg, S.M., McCarty, O.J. Quantitative Optical Microscopy: Measurement of Cellular Biophysical Features with a Standard Optical Microscope. *J. Vis. Exp.* (86), e50988, doi:10.3791/50988 (2014).

Abstract

We describe the use of a standard optical microscope to perform quantitative measurements of mass, volume, and density on cellular specimens through a combination of bright field and differential interference contrast imagery. Two primary approaches are presented: noninterferometric quantitative phase microscopy (NIQPM), to perform measurements of total cell mass and subcellular density distribution, and Hilbert transform differential interference contrast microscopy (HTDIC) to determine volume. NIQPM is based on a simplified model of wave propagation, termed the paraxial approximation, with three underlying assumptions: low numerical aperture (NA) illumination, weak scattering, and weak absorption of light by the specimen. Fortunately, unstained cellular specimens satisfy these assumptions and low NA illumination is easily achieved on commercial microscopes. HTDIC is used to obtain volumetric information from through-focus DIC imagery under high NA illumination conditions. High NA illumination enables enhanced sectioning of the specimen along the optical axis. Hilbert transform processing on the DIC image stacks greatly enhances edge detection algorithms for localization of the specimen borders in three dimensions by separating the gray values of the specimen intensity from those of the background. The primary advantages of NIQPM and HTDIC lay in their technological accessibility using "off-the-shelf" microscopes. There are two basic limitations of these methods: slow z-stack acquisition time on commercial scopes currently abrogates the investigation of phenomena faster than 1 frame/minute, and secondly, diffraction effects restrict the utility of NIQPM and HTDIC to objects from 0.2 up to 10 (NIQPM) and 20 (HTDIC) μm in diameter, respectively. Hence, the specimen and its associated time dynamics of interest must meet certain size and temporal constraints to enable the use of these methods. Excitingly, most fixed cellular specimens are readily investigated with these methods.

Video Link

The video component of this article can be found at https://www.jove.com/video/50988/

Introduction

The use of optical microscopy is now ubiquitous in the investigation of cellular organisms. Due to their low endogenous absorbance and weak scattering properties over the visible optical spectrum, cells do not strongly affect the amplitude of optical waves traversing them and thus appear semitransparent when imaged with standard bright field microscopes. Cellular specimens do, however, slow down optical waves traveling through them in a manner that is linearly related to the amount of local mass density in a particular region of space through which the light travels. Utilization of this heterogeneous time lag or "phase" profile of optical waves transmitted through microscopic specimens was first described in 1935 by Frits Zernike[1] and experimentally realized by Zernikein 1942[2]. Zernike was awarded the Nobel prize in 1953 for this achievement. Zeiss commercialized this modality in 1945[3]. In 1955, Smith and Nomarski would present their initial work on the use[4] and theory[5] of differential interference contrast (DIC) microscopy, a modality that uses the spatial gradient of phase as a contrast mechanism. DIC was commercialized by Zeiss in 1965in close collaboration with Nomarski[6]. In 1981, two laboratories demonstrated the first recorded live cell DIC imagery with the incorporation of video cameras into the optics train of the DIC microscope[7,8]. The era of live cell imaging was born.

Since this time, the execution of both phase contrast and DIC on commercial microscopes has largely been unchanged. These methods are principally utilized by biologists to produce images of cells for qualitative purposes: monitoring of morphology, tracking of subcellular structures, and investigations of membrane dynamics[9]. These techniques are qualitative in their "off-the-shelf" configuration as both phase and DIC images are arbitrary functions of the light source intensity, the illumination optics settings, and CCD camera gain, gamma, and exposure settings.

A small legion of physicists and optical engineers has endeavored to make commercial imaging modalities quantitative. Among the first efforts were two letters to *Nature* in 1952 and 1953 in which the physician-turned-biophysicist Robert Barer demonstrated the use of phase microscopy to determine cellular dry mass of cells by estimating phase shifts through these cell types using a commercially available phase microscope[10,11]. The field has developed a multitude of techniques over the ensuing years based around three basic label-free contrast

mechanisms: phase microscopy[10,11], DIC microscopy[12-17], and bright field[18-22] to determine optical path-length, phase, mass density, refractive index, and cellular volume.

In parallel, a large collection of custom optical instruments have also been developed since the 1950s, and have made far-reaching optical measurements ranging from applications in parasite growth[23], to documenting the cell cycle[24] to investigating membrane dynamics of red blood cells[25]. In particular, the past ten years has seen a wealth of label-free quantitative microscopy in the form of diffraction phase microscopy[26], tomographic phase microscopy[27], digital holographic microscopy[28], phase sensitive optical coherence microscopy[29], spatial light interference microscopy[30], Hilbert phase microscopy[31], and quantitative phase microscopy[32]. Despite their collective successes, these instruments have not been disseminated to the larger field of biological researchers owing, mostly, to their complex instrumentation and computational requirements.

Herein we describe the use of a standard optical microscope to perform quantitative measurements of mass, volume, and density on cellular specimens through a combination of bright field and DIC imagery. Two primary approaches are presented: noninterferometric quantitative phase microscopy (NIQPM), to perform measurements of total cell mass and subcellular density distribution, and Hilbert transform differential interference contrast microscopy (HTDIC), to determine volume. The primary advantages of NIQPM and HTDIC lay in their technological accessibility. The imaging conditions required for their successful execution are within the scope of normal operation of most commercially available microscopes. Additionally, the post-processing algorithms are stable, quick, and robust – having been implemented in MATLAB using fast Fourier transform (FFT) based algorithms whenever possible.

NIQPM is a method to reconstruct phase and the axially integrated mass density of cellular specimens from bright field imagery. Summation of this axially integrated mass density over the area of the specimen gives the total dry mass content of the specimen. The NIQPM protocol is based on the experimental foundations laid by Paganin and Nugent[18,19] – in which it was demonstrated that the phase profile of a cell could be reconstructed from through-focus bright field imagery of the sample – and the theoretical work of Frank, Altmeyer, and Wernicke[20] – on solving the paraxial wave models in an efficient FFT-based manner. The connection of phase to the dry mass density is based upon the work by Barer[10,11] and Popescu[33].

Volumetric information can be obtained from through-focus DIC imagery under high NA illumination conditions that enable optical sectioning of the specimen along the optical axis. Hilbert transform processing on the DIC image stacks greatly enhances edge detection algorithms for localization of the specimen borders in three dimensions by separating the gray values of the specimen intensity from those of the background. This work originates with Arinson *et al.*[34] although we have introduced both Fourier filtering methods to enhance contrast and a Sobel-based edge detection method for automated volumetric analysis of the sample. We have also validated HTDIC previously on polystyrene spheres ranging in size from the diffraction limit up to 20 μm in diameter[36].

While both NIQPM and HTDIC are technologically accessible owing to their development on commercial microscopes, the methods are fundamentally limited by the hardware configuration of the microscopes themselves. The primary limitations of these techniques are two-fold: slow z-stack acquisition time on commercial scopes, due to translation of the entire sample stage as opposed to just the objective lens, currently limits the investigation of phenomena faster than roughly 1 frame/minute, and secondly, diffraction effects restrict the utility of NIQPM and HTDIC to objects ranging in size from 0.2 up to 10 and 20 μm in diameter, respectively. Hence, the specimen and its associated time dynamics of interest must meet certain size and temporal constraints to enable the use of these methods on typical “off-the-shelf” instruments. Excitingly, most fixed cellular specimens are readily investigated with these methods.

An overview of the NIQPM and HTDIC protocols are given in **Figure 1**. In **Figure 2** we illustrate optimal and suboptimal through-focus imaging under both low and high NA illumination conditions for both bright field and DIC imagery. **Figures 3** and **4** demonstrate the parameter dependence of the NIQPM algorithm highlighting successful and unsuccessful implementations. **Figure 5** illustrates the steps involved in the HTDIC image-processing algorithm and demonstrates the optimal implementation of the algorithm to determine cellular volume.

Protocol

1. Microscope Specifications

To carry out imaging in the correct fashion the microscope should have the following specifications:

1. Possess both differential interference contrast (DIC) and brightfield (BF) contrast.
2. Have computer-controlled z-axis movement.
3. Have an adjustable aperture stop to vary the condenser lens numerical aperture. An aperture with a graded rule or electronic readout is required to know the value of the numerical aperture. The numerical aperture should range from 0.1 for NIQPM up to 0.9 (or higher) for HTDIC.
4. The microscope should have a narrow band color filter to be utilized for bright field imaging. This filter is required to fix the refractive increment, a wavelength-dependent facture used to convert phase to mass density for NIQP.

2. Differential Interference Contrast (DIC) Z-stack Acquisition

1. Open the SlideBook software and create a new slide for image collection.
2. Next, open the Focus Window. Under the **Filter Set** section, select **DIC**. On the **Scope** tab, under the **Condenser** section, adjust the **Aperture** slide bar to the furthest right position (open all the way). This provides high numerical aperture illumination and enhances optical sectioning of the specimen.
3. Focus on the sample using a DIC objective. Adjust the halogen lamp intensity until the sample is easily visible. To ensure the camera is not being saturated, select the Camera tab in the Focus Window and check that the histogram of pixel intensities is within the dynamic range of the camera.

4. Open the Image Capture window. In the **Capture Type** section, check the **3D** box. In the **3D Capture** section, select the **Range around center** and **Return to current location** boxes and specify the Z-direction range, number of planes, and step size. The Z-direction range should incorporate the entire sample.
5. In the **Filter Set** section of the Image Capture window, check the **DIC** box and specify exposure time. In the **Image Information** section, name the image (optional), and select **Start** to initiate the imaging.

3. Bright Field (BF) Z-stack Acquisition

1. Once the microscope has finished collecting the DIC Z-stack of the sample, open the Focus Window and select **Open** under the **Filter Set** section. Adjust the **Aperture** slide bar to the furthest left position (closed all the way) to provide low NA illumination.
2. Change the microscope light-path filter to green. Adjust the halogen lamp intensity until the sample is visible. Ensure there is no saturation of the camera by selecting the **Camera** tab in the Focus Window and checking that the histogram of pixel intensities is within the specified range.
3. Open the Image Capture window. The **3D Capture** settings from the DIC Z-stack acquisition will be displayed.
4. In the **Filter Set** section of the Image Capture window, check the **OPEN** box and specify exposure time. In the **Image Information** section, name the image (optional), and select **Start** to initiate Z-stack image acquisition.

4. Exporting Z-stack Images

1. Open a Z-stack capture. Change the view to 100%. Adjust the histogram of the pixel values to be displayed between 0 and the maximum pixel value of the camera (4,095 for 12 bit cameras, 65,535 for 16 bit.).
2. Select **View** > **Export** > **TIFF Series**. This will export the Z-stack as a series of TIFF images (one for each Z plane). Save the TIFF series in a separate folder with a name that has an underscore at the end (*i.e.* "DIC Stack 1_"). Repeat this with each DIC or BF Z-stack.

5. Volume Measurements

1. Open the HTDIC MATLAB program entitled "JoVE_HTDIC_v1.m".
2. Under Section 0 of the HTDIC program, update the dependencies directory variable. Copy and paste the directory containing the hilbert_transform_dic.m and sobel_edge_detect.m files from explorer (PC) in between the single quotes following "dependencies_directory =". ExecuteSection 0 of the JoVE_HTDIC_v1.m program.
3. In Section 1, update the "images_directory". Again, copy and paste the directory containing the through-focus images in .tif form in between the single quotes. ONLY RUN SECTION 1 ONCE.
4. Alignment and rotation of images for Hilbert transform Run Section 2 of the code. A dialog box titled "Define HTDIC Parameters" will appear. Five numbers are required from the user: the focal plane number where the DIC image of the sample is in focus, lateral resolution (μm/pixel in the image), the axial resolution (this is 0.1 for image acquisition in 0.1 μm axial steps), the rotation angle of the DIC image needed to perform the Hilbert transform, typical values are 45 and -135. Lastly, enter the region of interest size, this parameter defines the length of a side of a box that will subsequently appear - typical value is 400. Click **Ok**.
5. An image of the DIC focal plane specified by the focal plane number will appear with a blue box. Position the box over the feature of interest, *e.g.* a cell. The box need not be square. Once the box has been positioned over the desired region, double click inside the box.
6. Another figure will now appear: this figure contains a cropped and rotated image of the region of interest selected in the previous step. The contrast of the image should be such that dark features appear on the left while bright features appear on the right. Drag the blue box over the region of interest, reshape as necessary.
7. Section 3 generates a mask for the z-stack cube. There are two types of masks available: a rectangular mask to create a rectangle around the cell and a free-hand tool to outline the cell of interest by hand.
8. To generate a rectangular mask, uncomment line 167 and comment line 170 (comment a line out by placing a "%" at the beginning of that line). Execute Section 3 of the program. Click in the image and drag the mouse to begin defining the rectangular mask. Double click on the box to accept it.
9. To generate a hand-drawn mask, comment line 167 and uncomment line 170 and execute Section 3. Click and draw the desired mask with the mouse. Double click on the mask to accept it.
10. Run Section 4to construct the Hilbert transformed DIC image stack and the corresponding DIC image stack of the area of interest. The mask constructed in Section 3 will be applied to the Hilbert transform DIC stack and the regular DIC stack when "maskON" is set to 1 at line 179. Setting "maskON" to 0 will construct image stacks without applying the mask.
11. Run Section 5 to optimize the image segmentation of the xz cross sectional images of the region of interest. Figure 500, produced by the program, appears displaying three different types of contrast. The success of the algorithm to find the borders of the cell is reliant on a combination of the mask used and the value of "threshold" at line 229 of the program. Begin with a value of 0.5. Adjust the value of threshold and rerun this section of the program until the proper outlining is achieved in one of the columns.
12. If the outlining was best in column 1, use Section 6 to determine the volume using DIC image segmentation. If column 2 gave optimal results, run Section 7 to determine cell volume from Hilbert-transformed DIC imagery. If column 3 gave the optimal results, run Section 8 to determine volume using Fourier-filtered Hilbert-transformed DIC imagery.
13. The measured volume of the sample, reported in cubic μm (fl) is presented in the title of Figure 600, 700, or 800 produced by the program depending on which volume measurement is chosen.

6. Mass Measurements

1. Open the NIQPM MATLAB program entitled "JoVE_NIQPM_v1.m".
2. Under Section 0 of the NIQPM program, update the location of three directories needed to run the program. These are the "dependencies_directory," the "brightfield_directory," and the "dic_directory."

3. Next, run Section 1. This section of code generates a bright field image cube of the full field of the entire set of images. ONLY RUN SECTION 1 ONCE.
4. Next, run Section 2. A dialog box titled "Define NIQPM Parameters" will appear. Four numbers are required from the user: the focal plane number where the bright field image of the sample is in focus, lateral resolution (µm/pixel in the image), the axial resolution (this is 0.1 for image acquisition in 0.1 µm axial steps), and the region of interest size, this parameter defines the length of a side of a box that will subsequently appear - a typical value is 200. Click **Ok**.
5. An image of the bright field focal plane specified by the focal plane number will appear with a blue box.
    1. If the image is not in focus, double click in the blue box and rerun Section 2, be sure to adjust the focal plane number in the dialog box.
    2. If the image is in focus, drag the blue box around the image and resize it by selecting the nodes of the box and dragging them as necessary. Position the box around the feature of interest, *e.g.* a cell. The box need not be square. Double click inside the box to accept it.
6. Next, run Section 3 to construct a stack of bright field images cropped to the region of interest.
7. To generate the phase map, pseudo DIC image, and comparisons to bright field imagery and the true DIC image, run Section 4.
8. With the pseudo DIC and true DIC images as similar as possible the mass density map, total mass, and histogram of the cell density can be determined by running Section 5a or 5b. Section 5a carries out automated boarder detection of the field - optimize "threshold" at line 300 - typical values vary between 0.1-1. Rerun this section as needed to optimize the value of threshold. Section 5b carries out mass determination, *etc.* after the user outlines the cell of interest.

Representative Results

Correct sample illumination during through-focus image acquisition is critical to the successful implementation of the NIQPM **a**nd HTDIC algorithms. In **Figure 2** we illustrate low and high NA illumination under both DIC and bright field contrast for a polystyrene sphere and the human colorectal adenocarcinoma cell line SW620. **Figures 2A, 2C, 2I,** and **2K** demonstrate optimal imaging for NIQPM. **Figures 2F, 2H, 2N,** and **2P** demonstrate optimal imaging for HTDIC.

Figures 3 and **4** demonstrate the parameter dependence of the NIQPM algorithm highlighting both successful and unsuccessful implementations. In **Figure 3** we explore the phase profile of a 4.8 µm diameter polystyrene sphere - the expected profile is known theoretically and can thus be compared directly to the NIQPM reconstruction. **Figures 2I-L** present the best reconstruction obtainable for the sphere. Diffraction effects at both the boundaries of the sphere and inside prevent stable reconstruction at all points on the sphere. The central region of the sphere can be captured with NIQPM with a % error of 1-5%, **Figure 2L**.

Cellular specimens, whose phase properties are not known *a priori*, can be reconstructed using NIQPM in conjunction with a procedure to compare a "pseudo DIC" image - computed from the reconstructed phase - to an actual DIC image, determined from a direct optical measurement, of the cell. NIQPM has one free parameter - the plane in the bright field image stack at which the calculation is centered. This central focal plane should be adjusted until the pseudo DIC and true DIC images look as similar as possible. **Figures 4E-G** demonstrate an out-of-focus pseudo DIC image, an optimal pseudo DIC image, and the corresponding DIC image of the cell taken with an illumination NA of 0.9. Interestingly, the best phase map and corresponding pseudo DIC image do not necessarily correspond to an in focus bright field image, *viz*. **Figures 1A** and **1B**.

Lastly, **Figure 5** illustrates the steps involved in the HTDIC image-processing algorithm. From the DIC through-focus imagery under NA = 0.9 illumination, **Figures 5A** and **5D**, the Hilbert transform is preformed to remove the *bas relief* of the DIC images, **Figures 5B** and **5E**. This comes with some blurring along the optical axis that can be removed from high pass Fourier filtering, **Figures 5C** and **5F**. These final images are easily segmented to determine the area in each cross sectional plane of the specimen to infer the total cellular volume.

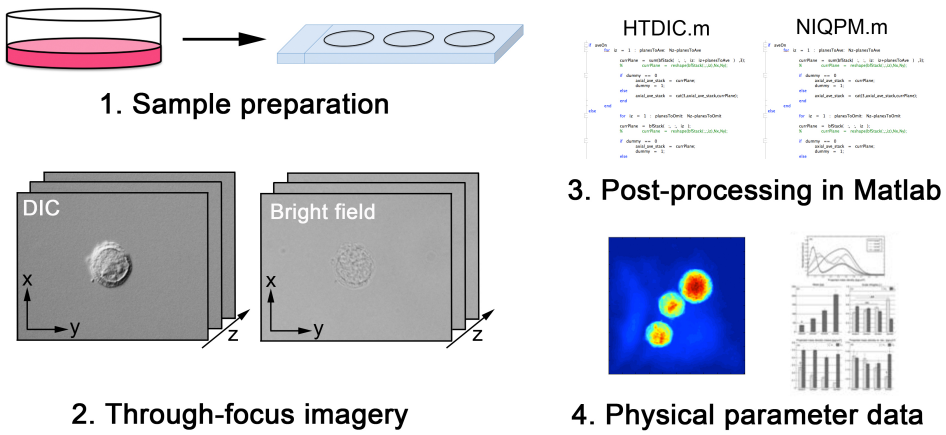

Figure 1. NIQPM and HTDIC Workflow. (**1.**) Microscopic specimens such as cells should be mounted on microscope slides with cover glass affixed over the sample using Fluoromount G. (**2.**) Through-focus images acquired under both DIC and bright field contrast with a standard "off-the-shelf" microscope form the input to the image processing algorithms. (**3.**) Post-processing of images in MATLAB to determine cell volume from DIC and cellular mass distribution from bright field imagery. (**4.**) Quantitative endpoint metrics: heat maps and bar graphs. Please click here to view a larger version of this figure.

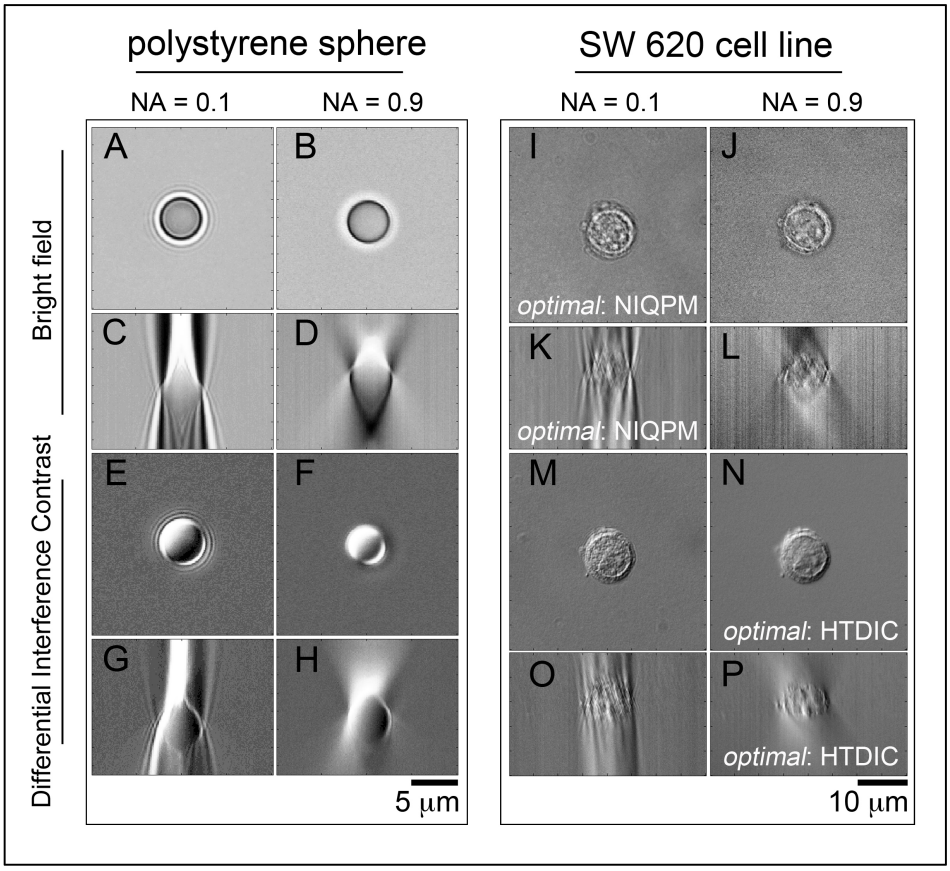

Figure 2. Through-focus DIC and bright field imagery of polystyrene spheres and SW620 cell lines. The optimal imaging conditions for NIQPM are bright field contrast with 0.1 NA illumination. For HTDIC DIC, 0.9 NA illumination is optimal. (**A**, **B**) *En face* bright field imagery of 4.8 μm diameter polystyrene sphere subject to 0.1 NA and 0.9 NA illumination, respectively. (**C**, **D**) Cross sectional bright field imagery of 4.8 μm diameter polystyrene sphere subject to 0.1 NA and 0.9 NA illumination, respectively. (**E**, **F**) *En face* DIC imagery of 4.8 μm diameter polystyrene sphere subject to 0.1 NA and 0.9 NA illumination, respectively. (**G**, **H**) Cross sectional DIC imagery of 4.8 μm diameter polystyrene sphere subject to 0.1 NA and 0.9 NA illumination, respectively. (**I**, **J**) *En face* bright field imagery of SW620 colorectal cancer cell line subject to 0.1 and 0.9 NA illumination, respectively. (**K**, **L**) Cross sectional bright field imagery of SW620 cell subject to 0.1 and 0.9 NA illumination, respectively. (**M**, **N**) *En face* DIC imagery of SW620 cell subject to 0.1 NA and 0.9 NA illumination, respectively. (**O**, **P**) Cross sectional DIC imagery of SW620 cell subject to 0.1 NA and 0.9 NA illumination. Please click here to view a larger version of this figure.

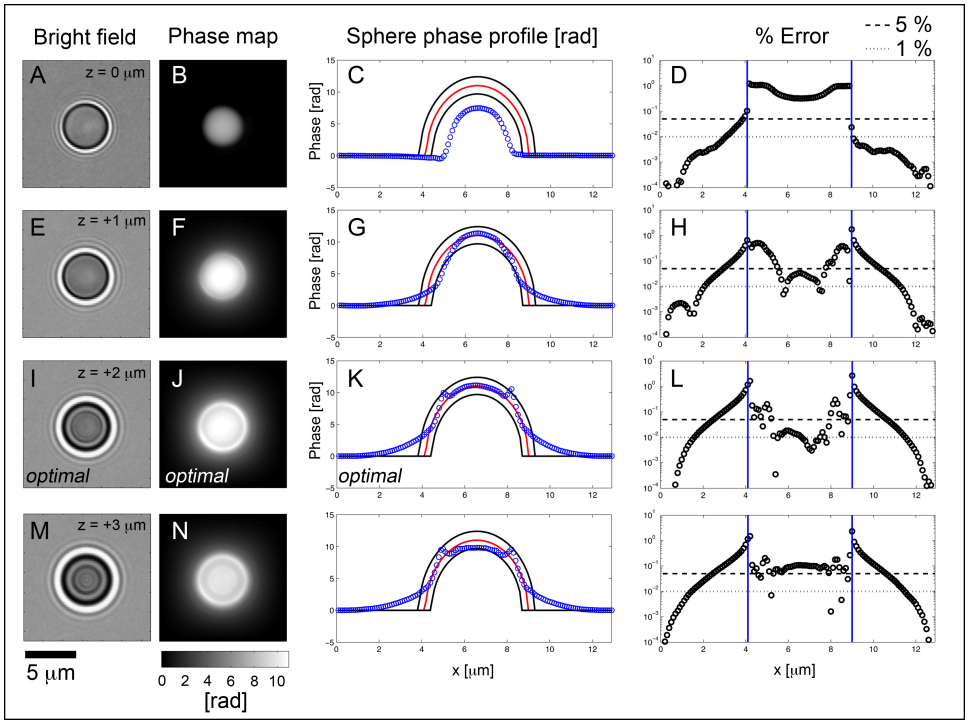

Figure 3. Optimal and suboptimal phase reconstructions:4.8 μm diameter polystyrene sphere. Each row investigates the focal plane dependence of the *en face* bright field intensity (first column) and the reconstructed phase profile as the focal plane begins at the midpoint through the sphere, z = 0, and moves past this plane in 1 μm steps. (**A**, **E**, **I**, **M**) *En face* bright field intensity, (**B**, **F**, **J**, **N**) corresponding phase reconstruction, (**C**, **G**, **K**, **O**) comparison of the reconstructed phase profile along the diagonal of the phase map, blue circles, theoretical phase profile, in red, and manufacturer's error tolerance, black lines, and (**D**, **H**, **L**, **P**) percent (%) error of the reconstructed phase with respect to the theoretical phase profile. Please click here to view a larger version of this figure.

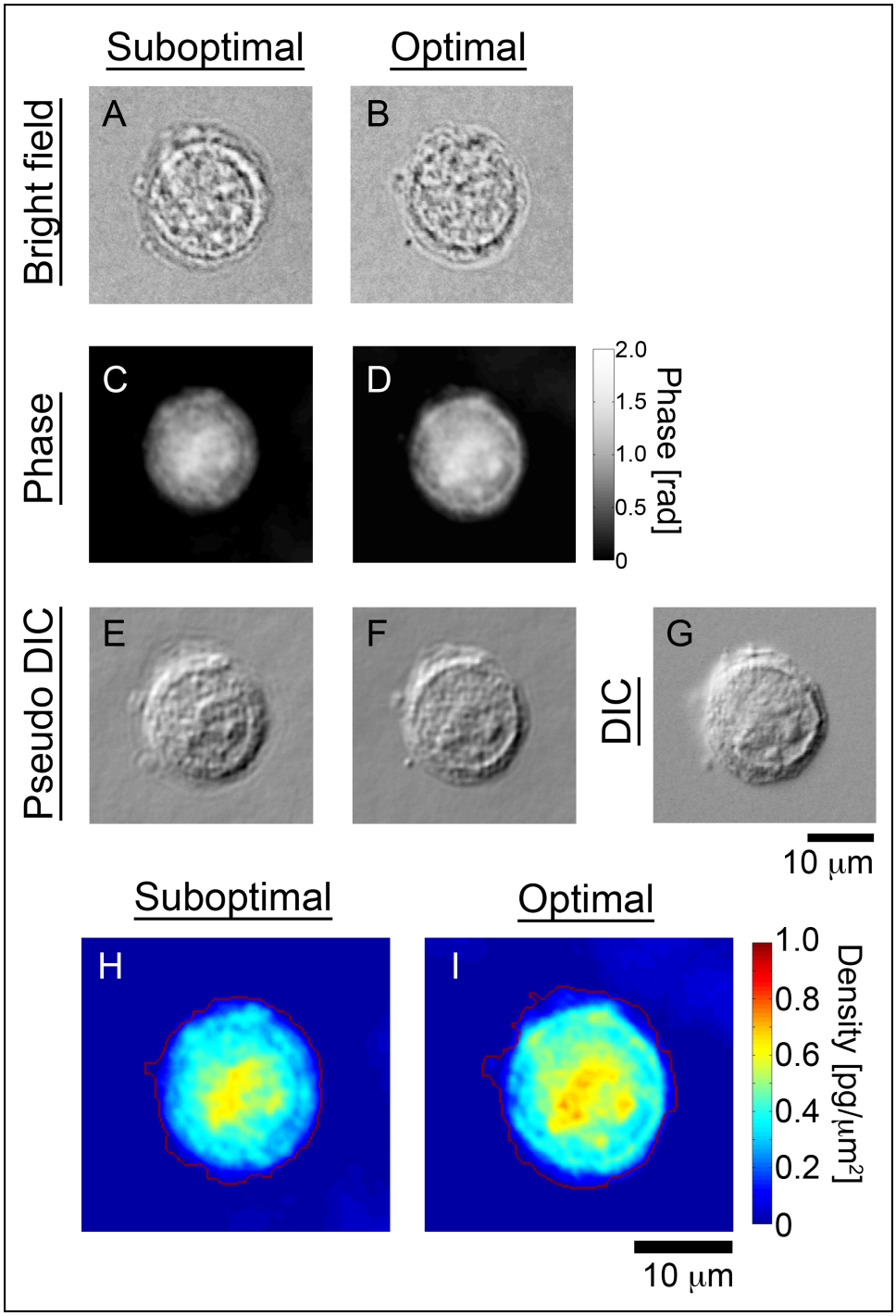

Figure 4. Optimal and suboptimal phase reconstructions: SW620 cell. The two columns compare suboptimal and optimal bright field image planes (**A**, **B**) from the z-stack to center the phase calculation. The corresponding phase reconstructions (**C**, **D**) are used to generate a pseudo DIC image (**E**, **F**). These are compared to the true DIC image, NA = 0.9 illumination, in (**G**). The pseudo DIC image best matching the DIC image determines the correct input images from the bright field image stack to use in phase reconstruction. Finally, phase is mapped to the projected mass density (**H**, **I**). Please click here to view a larger version of this figure.

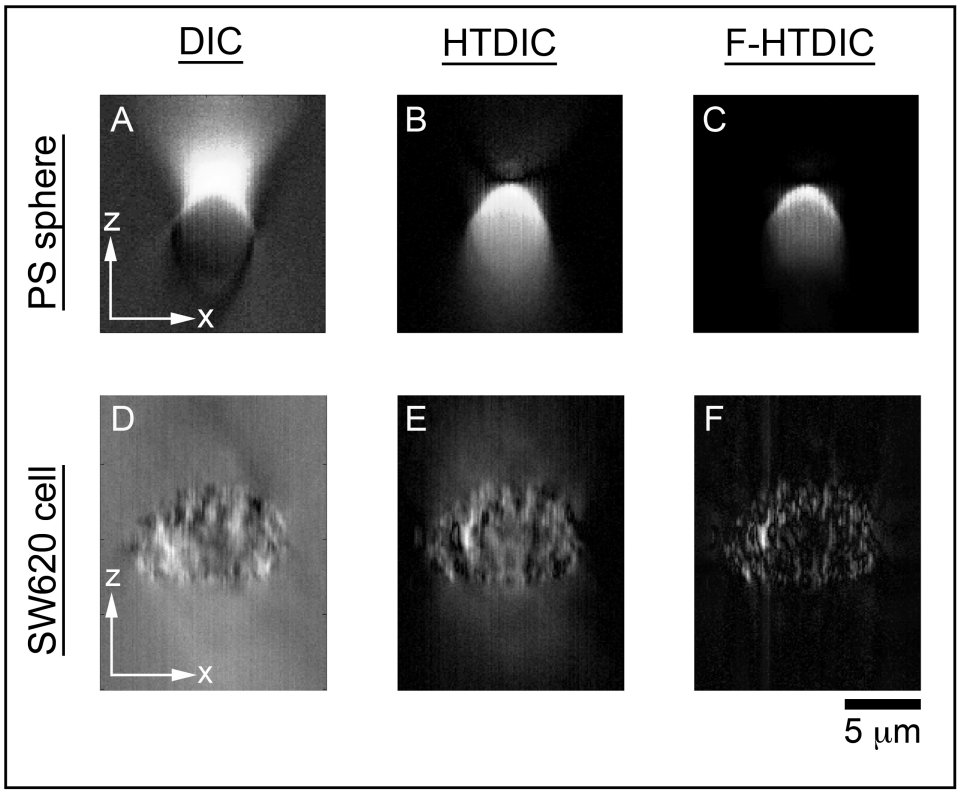

Figure 5. Optimal DIC contrast enhancement using HTDIC: polystyrene spheres and SW620 cell. (**A**) Cross-sectional DIC imagery of a 4.8 polystyrene sphere, (**B**) corresponding HTDIC image, (**C**) Fourier filtered HTDIC image. The axial dimension of the sphere images have been scaled to account for refractive index mismatch of the specimen (1.597) and the mounting media (1.4). (**D-F**) demonstrate the same image types for an SW620 cell, however, with no refractive index mismatch correction owing to the weak index contrast of the specimen. No thresholding has been performed on these images. Please click here to view a larger version of this figure.

Discussion

In general, NIQPM is a diffraction-limited technique validated on optical path-lengths ranging from 0.25-44.7. Validation was performed on n = 1.596 polystyrene spheres ranging in diameter from 0.11-9.8 μm suspended in Fluoromount G (data not shown). Cells possess optical path-lengths that range from nearly 0-7.

When measuring the density distribution of a specimen one may find that the pseudo DIC image looks fine while the density map possesses unwanted background contributions. This is due to noise in the bright field imagery of the sample used as the input to the NIQPM algorithm. Two possible modifications to the NIQPM method can be used to eliminate the unwanted background contributions: firstly, one may use longer exposure times to enhance signal-to-noise in the bright field imagery. This is especially critical when imaging optically thin specimens. Alternatively, one may reduce the axial spacing of the z-stack acquisition from 0.1-0.05 μm and average 2-3 planes together before inputting them into the NIQPM algorithm.

HTDIC based volume determination has been validated on polystyrene spheres ranging in diameter from 1-20 μm and has been cross-validated with confocal fluorescence microscopy[35]. The technique overestimates the volume of objects below the diffraction limit of the system due to diffraction effects associated with the point spread function of the optics.

Troubleshooting the HTDIC volume determination maybe required for small or thin specimens. The primary source of error comes from image segmentation using the built-in MATLAB Sobel-based edge detection used to determine the borders of the cell in the cross sectional images. The value of "threshold" in section 4 of the HTDIC program is critical in obtaining the best segmentation. Results tend to vary in a nonlinear way - with small changes in "threshold" drastically changing the enclosed area resulting from the edge detection. The current program presents the user with options to perform image segmentation from either the DIC z-stack, the HTDIC z-stack, or the F-HTDIC z-stack.

DIC alone is often better for large specimens while HTDIC and F-HTDIC work for smaller specimens (<5 μm in diameter).

A mask can enhance the ability of the method to segment the image. Section 2 allows the user to determine a mask to apply to the image cube. We recommend the use of a rectangular mask that truncates the horizontal (x-extent) of the cube while preserving the vertical (y-extent) of the cube.

In summary, NIQPM and HTDIC are technologically accessible quantitative imaging modalities that can be performed on standard "off-the-shelf" optical microscopes, in contrast to most existing methods. Central to these techniques is through-focus imagery of the sample under the appropriate imaging conditions: low NA illumination for NIQPM, and high NA illumination for HTDIC. The methods presented here can be generalized for use on systems other than those demonstrated here. The primary criteria required for these procedures is a microscope for which

the user has control over the z-movement of the stage and the ability to acquire images as the focal position of the objective lens is varied. The methods presented are suitable for imaging fixed cells or slowly moving biological specimens.

Disclosures

The authors have no financial interests in the work presented.

Acknowledgements

This work was supported by grants from the National Institutes of Health (U54CA143906 to K.G.P., O.J.T.M and R01HL101972 to O.J.T.M.) and an Oregon Medical Research Foundation Early Clinical Investigator Award (K.G.P.). O.J.T.M. is an American Heart Association Established Investigator (13EIA12630000). We thank Dr. Eric Anderson of the Knight Cancer Institute for preparing cell samples used in this work.

References

1. Zernike, F. Das Phasenkontrastverfahren bei der mikroskopischen Beobachtung, *Z. Technische Physik*. **16**, 454-457 (1935).
2. Zernike, F. Phase contrast, a new method for the microscopic observation of transparent objects. *Physica*. **9**, 974-986, 10.1016/S0031-8914(42)80079-8 (1942).
3. Blow, N. Finding Phase, *Nat. Cell Biol*. **11**, S6-S22, 10.1038/ncb1942 (2009).
4. Smith, F. H. Microscopic interferometry, *Research*. **8**, 385-395 (1955).
5. Nomarski, G. Microinterféromètre différentiel à ondes polarisées, *J. Phys. Radium*. **16**, 9S-11S (1955).
6. Lang, W. Nomarski differential-interference contrast microscopy, *Zeiss Inform*. **70**, 114-120, http://zeiss-campus.magnet.fsu.edu/referencelibrary/basics/dic.html (1968).
7. Allen, R. D., Allen, N. S., Travis, J. L. Video-enhanced contrast, differential interference contrast (VEC-DIC) microscopy: a new method capable of analyzing microtubule-related motility in the reticulopodial network of *Allogromia laticollaris*. *Cell Motil. Cytoskel*. **1**, 291-302, 10.1002/cm.970010303 (1981).
8. Inoué, S. Video image processing greatly enhances contrast, quality, and speed in polarization-based microscopy. *J. Cell Biol*. **89**, 346-356, 10.1083/jcb.89.2.346 (1981).
9. Aslan, J.E., Itakura, A., Gertz, J.M., McCarty, O.J. Platelet shape change and spreading. *Methods Mol. Biol*. 10.1007/978-1-61779-307-3_7 (2012).
10. Barer, R. Interference microscopy and mass determination. *Nature*. 169, 366-367, 10.1038/169366b0 (1952).
11. Barer, R. Ross, K. F. A. Tkaczyk, S. Refractometry of living cells. *Nature*. **171**, 720-724, 10.1038/171720a0 (1953).
12. Preza, C., Snyder, D.L., Conchello, J.A. Theoretical development and experimental evaluation of imaging models for differential interference contrast microscopy. *J. Opt. Soc. Am. A*. **16**, 2185-2199, 10.1364/JOSAA.16.002185 (1999).
13. Arnison, M. R., Larkin, K. G., Sheppard, C. J., Smith, N. I., Cogswell, C. J. Linear phase imaging using differential interference contrast microscopy. *J. Microsc*. **214**, 7-12, 10.1111/j.0022-2720.2004.01293.x (2004).
14. Van Munster, E. B., Van Vliet, L. J., Aten, J. A. Reconstruction of optical pathlength distributions from images obtained by a wide#field differential interference contrast microscope. *J. Microsc*. **188**, 149-157 (1997).
15. Kou, S. S., Waller, L., Barbastathis, G., Sheppard, C. J. Transport-of-intensity approach to differential interference contrast (TI-DIC) microscopy for quantitative phase imaging. *Opt. Lett*. **35**, 447-449, 10.1364/OL.35.000447 (2010).
16. Xu, M., Scattering-phase theorem: anomalous diffraction by forward-peaked scattering media. *Opt. Exp*. **19**, 21643-21651, 10.1364/OE.19.021643 (2011).
17. Duncan, D. D., Fischer, D. G., Dayton, A., Prahl, S. A. Quantitative Carré differential interference contrast microscopy to assess phase and amplitude. *J. Opt. Soc. Am. A*. **28**, 1297-1306, 10.1364/JOSAA.28.001297 (2011).
18. Barty, A., Nugent, K. A., Paganin, D., Roberts, A. Quantitative optical phase microscopy. *Opt. Lett*. **23**, 817-819, 10.1364/OL.23.000817 (1998).
19. Paganin D.; Nugent, K. A. Non-interferometric phase imaging with partially coherent light. *Phys. Rev. Lett*. **80**, 2586-2589, 10.1103/PhysRevLett.80.2586 (1998).
20. Frank, J., Altmeyer, S., Wernicke, G. Non-interferometric, non-iterative phase retrieval by Green's functions. *J. Opt. Soc. Am. A* **27**, 2244-2251, 10.1364/JOSAA.27.002244 (2010).
21. Phillips, K. G., Velasco, C. R., Li, J., Kolatkar, A., Luttgen, M., Bethel, K., Duggan, B., Kuhn, P., McCarty, O.J. Optical quantification of cellular mass, volume, and density of circulating tumor cells identified in an ovarian cancer patient. *Front. Oncol*. **2**, 72, 1-8, 10.3389/fonc.2012.00072 (2012).
22. Phillips, K. G., Jacques, S. L., McCarty, O. J. Measurement of single cell refractive index, dry mass, volume, and density using a transillumination microscope. *Phys. Rev. Lett*. **109**, 118105, 1-5, 10.1103/PhysRevLett.109.118105 (2012).
23. Park, Y. K., Diez-Silva, M., Popescu, G., Lykotrafitis, G., Choi, W., Feld, M.S., Suresh, S. Refractive index maps and membrane dynamics of human red blood cells parasitized by Plasmodium falciparum. *Proc. Natl. Acad. Sci. U.S.A*. **105**,13730-13735, 10.1073/pnas.0806100105 (2008).
24. Mir, M., Wang, Z., Shen, Z., Bednarz, M., Bashir, R., Golding, I., Popescu, G. Optical measurement of cycle-dependent cell growth. *Proc. Natl. Acad. Sci. U.S.A*. **108**, 13124-13129, 10.1073/pnas.1100506108 (2011).
25. Popescu, G., Ikeda, T., Goda, K., Best-Popescu, C. A., Laposata, M., Manley, S., Feld, M. S. Optical measurement of cell membrane tension. *Phys. Rev. Lett*. **97**, 218101, 1-4, 10.1103/PhysRevLett.97.218101 (2006).
26. Popescu, G., Ikeda, T., Dasari, R. R., Feld, M. S. Diffraction phase microscopy for quantifying cell structure and dynamics. *Opt. Lett*. **31**, 775-777, 10.1364/OL.31.000775 (2006).
27. Choi, W., Fang-Yen, C., Badizadegan, K., Oh, S., Lue, N., Dasari, R. R., Feld, M. S. Tomographic phase microscopy. *Nat. Methods*. **4**(9), 717-719, 10.1038/nmeth1078 (2007).

28. Charrière, F., Marian, A., Montfort, F., Kuehn, J., Colomb, T., Cuche, E., Depeursinge, C. Cell refractive index tomography by digital holographic microscopy. *Opt. Lett*. **31**, 178-180, 10.1364/OL.31.00017, (2006).
29. Joo, C., Akkin, T., Cense, B., Park, B. H., de Boer, J. F. Spectral-domain optical coherence phase microscopy for quantitative phase-contrast imaging. *Opt. Lett*. **30**, 2131-2133, 10.1364/OL.30.002131 (2005).
30. Wang, Z., Millet, L., Mir, M., Ding, H., Unarunotai, S., Rogers, J., Popescu, G. Spatial light interference microscopy (SLIM). *Opt. Exp*. **19**, 1016-1026, 10.1364/OE.19.001016 (2011).
31. Ikeda, T., Popescu, G., Dasari, R. R., Feld, M. S. Hilbert phase microscopy for investigating fast dynamics in transparent systems. *Opt. Lett*. **30**, 1165-1167, 10.1364/OL.30.001165 (2005).
32. Shaked, N. T., Rinehart, M. T., Wax, A. Dual-interference-channel quantitative-phase microscopy of live cell dynamics. *Opt. Lett*. **34**, 767-769, 10.1364/OL.34.000767 (2009).
33. Popescu, G.; Park, Y., Lue, N., Best-Popescu, C., Deflores, L., Dasari, R. R., Badizadegan, K. Optical imaging of cell mass and growth dynamics. *Am. J. Physiol. Cell Physiol*. **295**, C538-C544, 10.1152/ajpcell.00121.2008 (2008).
34. Arnison, M. R., Cogswell, C. J., Smith, N. I., Fekete, P. W., Larkin, K. G. Using the Hilbert transform for 3D visualization of differential interference contrast microscope images, *J. Microsc*. **199**, 79-84, 10.1046/j.1365-2818.2000.00706.x (2001).
35. Baker, S. M., Phillips, K. G., McCarty, O. J. Development of a label-free imaging technique for the quantification of thrombus formation. *Cell. Mol. Bioeng*. **5**, 488-492, 10.1007/s12195-012-0249-4 (2012).

